Collectively induced exceptional points of quantum emitters coupled to nanoparticle surface plasmons

Po-Chen Kuo [1], Neill Lambert [2], Adam Miranowicz [2,3], Hong-Bin Chen [4,5,*], Guang-Yin Chen [6,†], Yueh-Nan Chen [1,5,‡] and Franco Nori [2,7]

[1]*Department of Physics, National Cheng Kung University, Tainan 70101, Taiwan*
[2]*Theoretical Quantum Physics Laboratory, RIKEN Cluster for Pioneering Research, Wako-shi, Saitama 351-0198, Japan*
[3]*Faculty of Physics, Adam Mickiewicz University, 61-614 Poznań, Poland*
[4]*Department of Engineering Science, National Cheng Kung University, Tainan 70101, Taiwan*
[5]*Center for Quantum Frontiers of Research & Technology, NCKU, Tainan 70101, Taiwan*
[6]*Department of Physics, National Chung Hsing University, Taichung 40227, Taiwan*
[7]*Department of Physics, The University of Michigan, Ann Arbor, Michigan 48109-1040, USA*

Exceptional points, resulting from non-Hermitian degeneracies, have the potential to enhance the capabilities of quantum sensing. Thus, finding exceptional points in different quantum systems is vital for developing such future sensing devices. Taking advantage of the enhanced light-matter interactions in a confined volume on a metal nanoparticle surface, here we theoretically demonstrate the existence of exceptional points in a system consisting of quantum emitters coupled to a metal nanoparticle of subwavelength scale. By using an analytical quantum electrodynamics approach, exceptional points are manifested as a result of a strong-coupling effect and observable in a drastic splitting of originally coalescent eigenenergies. Furthermore, we show that exceptional points can also occur when a number of quantum emitters are collectively coupled to the dipole mode of localized surface plasmons. Such a quantum collective effect not only relaxes the strong-coupling requirement for an individual emitter, but also results in a more stable generation of the exceptional points. Furthermore, we point out that the exceptional points can be explicitly revealed in the power spectra. A generalized signal-to-noise ratio, accounting for both the frequency splitting in the power spectrum and the system's dissipation, shows clearly that a collection of quantum emitters coupled to a nanoparticle provides a better performance of detecting exceptional points, compared to that of a single quantum emitter.

I. INTRODUCTION

The rapid development of quantum technologies has triggered intense interest in the potential of quantum sensors [1,2]. Without considering energy loss or gain, one only needs a Hermitian Hamiltonian to describe an energy-conserving system, where a diabolical point (DP) [3], containing degenerate eigenenergies with different corresponding eigenvectors, may be found. In realistic systems, however, one must consider the energy exchange process with an environment [4], which in some situations can be described by an effective non-Hermitian Hamiltonian.

An intriguing property of non-Hermitian Hamiltonians is that the degeneracy of eigenenergies can occur alongside the coalescence of the corresponding eigenstates, i.e., the occurrence of exceptional points (EPs) [5,6]. Owing to different mathematical properties of DPs and EPs, when the system is subject to a perturbation, the resulting energy splitting of a spectrum is shown to follow a square-root dependence on

the perturbation at an EP, instead of being linearly proportional to the perturbation, as occurs at a DP [6–8]. In other words, the energy splitting of the spectrum at an EP may have an extremely sensitive dependence on the parametric change caused even by a small perturbation. This is why the splitting near an EP may be exploited for ultrasensitive sensing [6,9,10].

We note, however, that the true applicability and usefulness of EP sensing depend on the details of how the parametric change is measured [8,11]. In any case, finding practically useful EPs in physically accessible systems [12–14] and parameter regimes is still an open problem [15–17], and a range of candidates have been studied, such as parity-time-symmetric systems [12,18–25], coupled atom-cavity systems [26], microcavities [12,20,21,27–29], microwave cavities [30–33], acoustic systems [34], photonic lattices [19,35], photonic crystal slabs [36], exciton-polariton billiards [37], plasmonic nanoresonators [38], ring resonators [39], optical resonators [40–42], and topological arrangements [37].

However, the typical size of these systems possessing EPs is usually too large (of several hundred nanometers) to be utilized for sensing in some important applications. Nevertheless, for such a nanoscale, the relevant parameters, such as coupling strength between objects, do not easily reach

*hongbinchen@gs.ncku.edu.tw
†gychen@phys.nchu.edu.tw
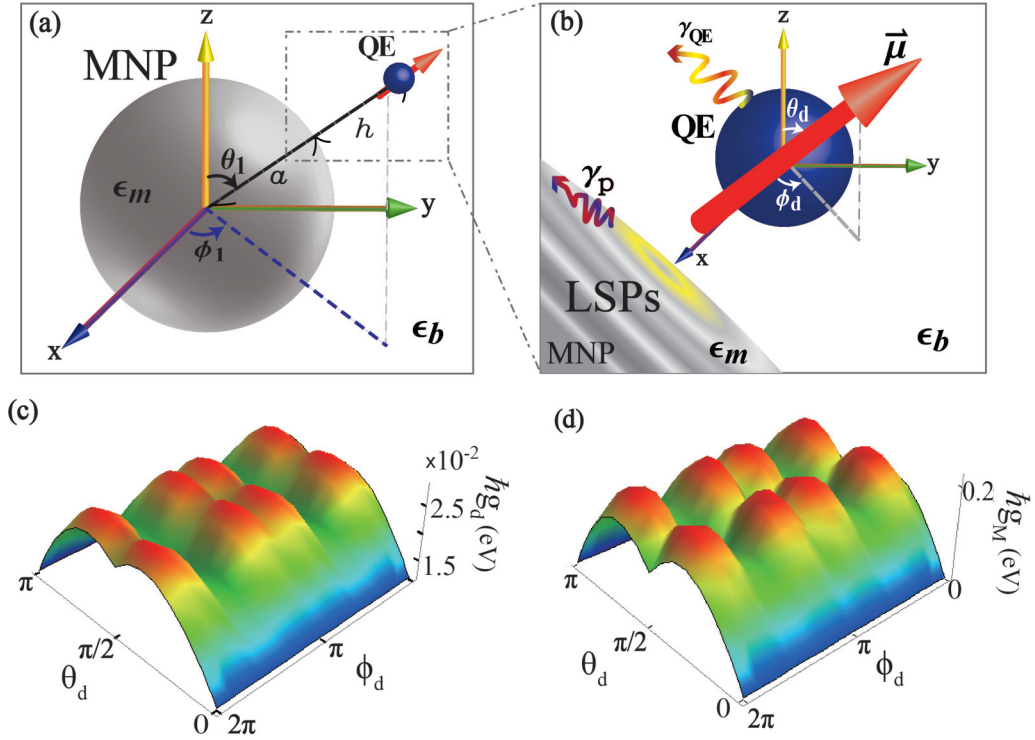‡yuehnan@mail.ncku.edu.tw

FIG. 1. Schematic diagram of the QE-MNP model in spherical coordinates, and examples of the the strength of the coupling to the dipole mode and pseudomode with different dipole moment orientations. (a) A single quantum emitter embedded in a dielectric medium with permittivity ϵ_b is in proximity to a silver metal nanoparticle at the position (r_1, θ_1, ϕ_1), where $r_1 = a + h$. (b) Partial enlargement of (a): A quantum emitter with the dipole orientation $\vec{\mu} = (\mu_r, \mu_\theta, \mu_\phi)$ coupled to the localized surface plasmons with damping rate γ_p as well as other decay channels, such as internal nonradiative decay and spontaneous decay into the dielectric material, with a total rate γ_{QE}. (c, d) The strengths of the coupling to the dipole mode $\hbar g_d$ (c) and to the pseudomode $\hbar g_M$ (d), as functions of θ_d and ϕ_d with $h = 1$ nm.

the requirement of forming an EP. Fortunately, when light is incident on a metal nanoparticle (MNP), local oscillations of electrons, known as localized surface plasmons (LSPs), can occur at a length scale much smaller than the wavelength of light [43–46]. This implies that by placing quantum emitters (QEs), such as biomolecules, near an MNP the electromagnetic (EM) field outside the MNP becomes tightly localized around the metal surface, giving rise to possible strong couplings between the QEs and the MNP [47–49]. Under suitable dissipation conditions, the existence of EPs at a subwavelength scale becomes possible.

In this paper, we first predict the existence of an EP in the case of an MNP coupled to a QE, which is generically described as a two-level system. The role of the QE can be played by, e.g., a biochemical molecule or a quantum dot. Surprisingly, we find that the EP can also occur when several QEs are collectively coupled to the dipole mode in the MNP. Such a quantum collective effect not only relaxes the strong-coupling requirement for the individual QE, but also results in more feasible conditions to generate an EP. Additionally, by implementing a photon detector near the QE-MNP system, we show that the observation of an EP, as well as the frequency splittings in the power spectrum, are experimentally accessible.

Moreover, we analyze how accurately an EP can be detected by comparing frequency splitting in theoretical eigenenergy spectra and the output power spectra. Note that the required accuracy of the observation of an EP is limited by

dissipation. To specify the degree to which the occurrence of an EP is affected by dissipation, we propose to use the signal-to-noise ratio (SNR) taking into account both frequency splitting and dissipation. From our analysis of the signal-to-noise ratio, we conclude that a collection of QEs coupled to an MNP provides a better performance of the detection of EPs compared to that of a single QE.

II. SINGLE QUANTUM EMITTER COUPLED TO THE SILVER NANOPARTICLE

In order to explore the possibility of using the emitter-plasmon system as a quantum sensor, we follow the formalism of Ref. [48]. Thus, we first consider a composite system embedded in a nondispersive, lossless dielectric medium with permittivity of $\epsilon_b = 2.3$, composed of a two-level QE close to the surface of a silver MNP with a distance h, as depicted in Fig. 1(a). The MNP with a radius $a = 7$ nm can be characterized by a Drude-type permittivity $\epsilon_m = \epsilon_\infty - \omega_p^2/[\omega(\omega + i\gamma_p)]$ with $\epsilon_\infty = 4.6$, $\hbar\omega_p = 9$ eV, and the dissipation of silver $\hbar\gamma_p = 0.1$ eV. Here, the QE acts as a pointlike dipole with the distance h larger than 1 nm [50]. As shown in Fig. 1(b), $\vec{\mu} = (\mu_r, \mu_\theta, \mu_\phi)$ is the dipole moment of the QE in the spherical coordinates. The strength of the dipole moment is $|\vec{\mu}| = 0.38\, e$ nm [48].

The Hamiltonian of the QE is given by $\hat{H}_{QE} = \hbar[\omega_0 - i(\gamma_{QE}/2)]\hat{\sigma}_{e_1,e_1}$, where $\sigma_{e_1,e_1} = |e_1\rangle\langle e_1|$, $|e_1\rangle$ is the excited state, and $\hbar\omega_0$ is the transition energy. Here, the

Hamiltonian of the EM field can be expanded in terms of the annihilation (creation) operators of the radiation field, $\hat{f}(\vec{r}, \omega)$ [$\hat{f}^{(\dagger)}(\vec{r}, \omega)$], including all the EM modes of the vacuum and LSPs as $\hat{H}_{EM} = \int d^3\vec{r} \int_0^\infty d\omega \hbar\omega \hat{f}^\dagger(\vec{r}, \omega)\hat{f}(\vec{r}, \omega)$. When excited, the QE is not only coupled electromagnetically to the LSPs on the metal surface, but also coupled to several decay channels, such as internal nonradiative decay due to rovibrational or phononic effects and spontaneous decay into the dielectric material, with a total rate γ_{QE}. The interaction between the QE and EM modes is given by $\hat{H}_{int} = -\int_0^\infty d\omega\{\vec{\mu} \cdot [\hat{E}(\vec{r}, \omega)\hat{\sigma}_+^{(1)} + \text{H.c.}]\}$, where $\hat{\sigma}_+^{(1)} = |e_1\rangle\langle g_1|$ represents the raising operator and

$$\hat{E}(\vec{r}, \omega) = i\sqrt{\frac{\hbar}{\pi\epsilon_0}}\frac{\omega^2}{c^2}\int d^3\vec{r}_1\sqrt{\epsilon^I(\vec{r}_1, \omega)}\widehat{G}(\vec{r}, \vec{r}_1, \omega)\hat{f}(\vec{r}_1, \omega)$$

represents the quantized EM field [51]. Here, $\epsilon^I(\vec{r}_1, \omega)$ is the imaginary part of $\epsilon(\vec{r}_1, \omega)$, and H.c. stands for the Hermitian conjugate. Note that $\widetilde{G}(\vec{r}, \vec{r}_1, \omega)$ represents the dyadic Green's function obtained from the Maxwell-Helmholtz wave equation under the boundary condition

$$\nabla \times \nabla \times \widetilde{G}(\vec{r}, \vec{r}_1, \omega) - \frac{\omega^2}{c^2}\epsilon(\vec{r}, \omega)\widetilde{G}(\vec{r}, \vec{r}_1, \omega) = \mathbf{I}\delta(\vec{r}, \vec{r}_1), \quad (1)$$

where $\mathbf{I}$ stands for the unit dyad. In this regard, the Green's function, which contains all the information about the EM field in both dielectric and metal media, plays a prominent role in the realization of the coherent coupling between the QE and the MNP. Therefore, this QE-MNP system can then be described by the total Hamiltonian, within the rotating-wave approximation, as $\hat{H} = \hat{H}_{QE} + \hat{H}_{EM} + \hat{H}_{int}$. For a single quantum excitation, let $C_1(t)$ denote the probability amplitude that the QE can be excited. By solving the Schrödinger equation, one can obtain the following integrodifferential equation for $C_1(t)$ [52]:

$$\frac{d}{dt}C_1(t) = -\int_0^t dt_1 \int_0^\infty d\omega J(\omega)e^{i(\omega_0 - \omega)(t - t_1)}C_1(t_1), \quad (2)$$

where $J(\omega)$ is the so-called spectral density of the QE-MNP system, which can be expanded into the sum of Lorentzian distributions (see the Appendix):

$$J(\omega) \approx \sum_{n=0}^\infty \frac{g_n^2}{\pi}\frac{\gamma_p/2}{(\omega - \omega_n)^2 + (\gamma_p/2)^2}, \quad (3)$$

where

$$g_n^2 = \sum_{\alpha=r,\theta,\phi} g_{n\alpha}^2, \quad (4)$$

with

$$\omega_n = \omega_p/\sqrt{\epsilon_\infty + \epsilon_d(n + 1)/n}$$

being the cutoff frequency of the LSPs characterized by the angular momentum n and the Ohmic loss γ_p. Suppose that there is no direct tunneling between the MNP and the QE ($h > 1$ nm). Then the coupling strengths between the QE and the Lorentzian modes of the LSPs are given by

$$g_{nr}^2 = \mu_r^2(n + 1)^2 f_n(\omega_n) \quad (5)$$

and

$$g_{n\theta(\phi)}^2 = \mu_{\theta(\phi)}^2 \sum_{m=0}^n \mathcal{D}_{nm}[mP_n^m(0)]^2 f_n(\omega_n), \quad (6)$$

where

$$\mathcal{D}_{nm} = (2 - \delta_{m0})\frac{(n - m)!}{(n + m)!},$$

δ_{m0} is the Kronecker delta function,

$$f_n(\omega_n) = \frac{a^{2n+1}}{(a + h)^{2n+4}}\left(1 + \frac{1}{2n}\right)\frac{\omega_p}{4\pi\epsilon_0\hbar}\left(\frac{\omega_n}{\omega_p}\right)^3,$$

and $P_n^m(x)$ is the associated Legendre polynomial. In order to properly evaluate and fit the polarization spectrum, the LSPs on the MNP can be approximately separated into the dipole mode and the pseudomode [53,54] with cutoff frequencies [48] $\omega_d = \omega_1$ and

$$\omega_M = \frac{\sum_{n=2}^\infty \omega_n g_n^2}{\sum_{n=2}^\infty g_n^2}$$

correspondingly. The couplings to the dipole mode and pseudomode are $g_d = g_1$ and $g_M^2 = \sum_{n=2}^\infty g_n^2$, respectively.

Typically, the coupling to the pseudomode can be neglected when h is large enough. However, when the QE is placed closer to the MNP with $h \leqslant 10$ nm, the coupling to the pseudomode can play a dominant role, even five to ten times stronger than the one to the dipole mode. In addition to h, both the coupling strengths, g_d and g_M, also depend on the orientation of the transition dipole moment, as shown in Figs. 1(c) and 1(d).

This QE-MNP system can formally be described by a non-Hermitian three-level Hamiltonian revealing EPs [48]:

$$\hat{H}_{3\times3} = \begin{bmatrix} \omega_0 - i\frac{\gamma_{QE}}{2} & g_d & g_M \\ g_d & \omega_d - i\frac{\gamma_p}{2} & 0 \\ g_M & 0 & \omega_M - i\frac{\gamma_p}{2} \end{bmatrix}. \quad (7)$$

When the QE is gradually moved closer to the MNP, both imaginary and real parts of the eigenenergies coalesce at a certain distance, resulting in the emergence of the EP. As shown in Figs. 2(a) and 2(b), we can observe the EP while placing the QE at $h \approx 3$ nm with the dipole moment orientation $(\mu, \theta_d, \phi_d) = (0.38, \pi/2, 0)$.

Due to the huge difference in the magnitudes, the appearance of an EP mainly results from the coupling between the QE and the pseudomode instead of the dipole mode. Consequently, to investigate the circumstance in which the EP forms, we consider a reduced Hamiltonian as well [26,38]:

$$\hat{H}_{2\times2} = \begin{bmatrix} \omega_0 - i\frac{\gamma_{QE}}{2} & g_M \\ g_M & \omega_M - i\frac{\gamma_p}{2} \end{bmatrix}, \quad (8)$$

which describes the relevant coupling between the QE and the pseudomode; furthermore, it is a standard form of Hamiltonians generically studied in the context of EPs [6,26,38]. It is clear that the EP can arise only under the conditions $\omega_0 = \omega_M$ and $g_M = (\gamma_p - \gamma_{QE})/4$.

In the vicinity of the EP shown in Fig. 2, the real parts of the eigenenergies drastically split when the QE is placed even closer to the MNP. It is noteworthy that, in the region where
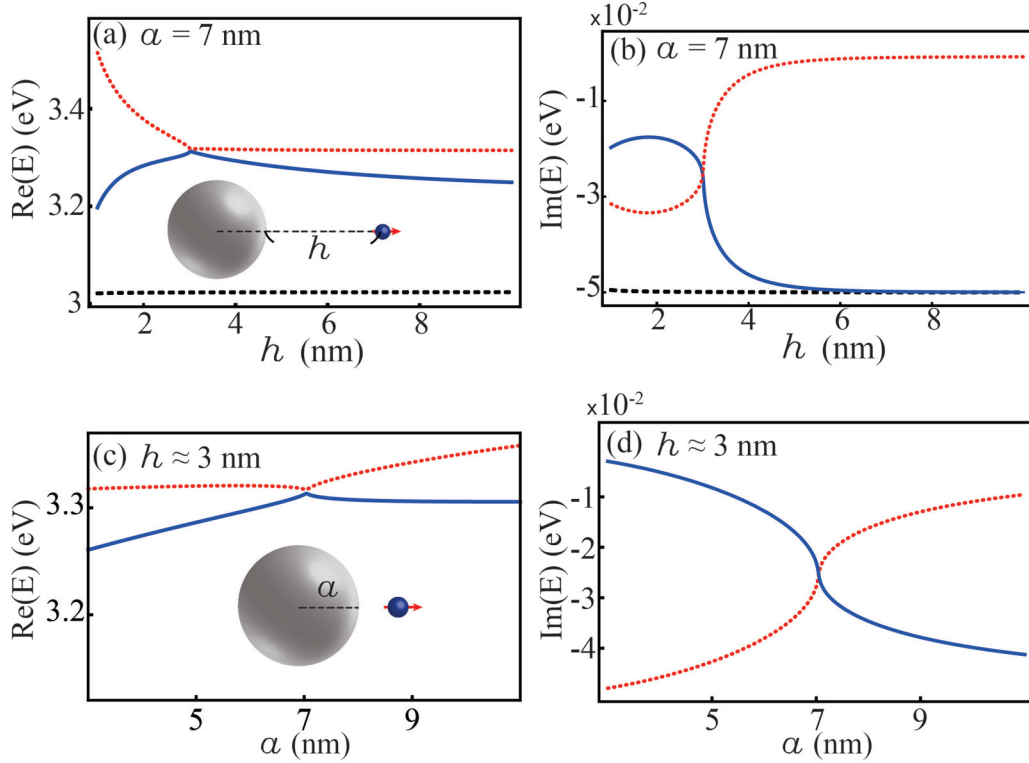
FIG. 2. Dependence of the eigenenergies of $H_{3\times3}$ on the distance h and the metal nanoparticle radius a. The dipole moment orientation is fixed at $(\mu, \theta_d, \phi_d) = (0.38, \pi/2, 0)$ for the following calculations. (a) Real and (b) imaginary parts of the energy spectra jointly show the appearance of an exceptional point when placing the quantum emitter at $h \approx 3$ nm. The occurrence of the eigenenergy splittings in the real (imaginary) part of the region, $h > 3$ ($h < 3$), is caused by both the detuning ($\omega_M - \omega_0$) and the coupling to the dipole mode. (c), (d) Real (c) and imaginary (d) parts of energy spectra as a function of the metal nanoparticle radius a showing an exceptional point.

$h > 3$, splitting occurs as well, in contrast to the conventional coalescence observed in the previous literature [5,6,26]. These splittings are consequences of the off-resonance condition $\omega_0 \neq \omega_M$ due to the dependence of ω_M on h. Additionally, the coupling between the dipole mode and the QE also induces splitting. By solving the eigenvalue of $\hat{H}_{3\times3}$ in Eq. (7), the splitting strength $\triangle E$, i.e., the difference between the dotted red and solid blue eigenenergies in Fig. 2, close to the EP can be analytically given by

$$\triangle E = \frac{-\sqrt{3}i[u^2 + p(\omega_d, g_d)^{2/3} - 48g_d^2]}{12p(\omega_d, g_d)^{1/3}}, \quad (9)$$

where

$$p(\omega_d, g_d) = 144g_d^2(2\omega_{d\triangle} + i\gamma_\triangle) + iu^3 + 12q(\omega_d, g_d), \quad (10)$$

$$q(\omega_d, g_d) = -96g_d^4(\gamma_\triangle^2 - 10i\gamma_\triangle\omega_{d\triangle} + 2\omega_{d\triangle}^2) \\ - 3\gamma_\triangle g_d^2 u^3 - 768g_d^6, \quad (11)$$

$u = \gamma_\triangle + 4i\omega_{d\triangle}$, $\omega_{d\triangle} = \omega_d - \omega_0$, and $\gamma_\triangle = \gamma_p - \gamma_{QE}$. With Eq. (9), one can evaluate how the dipole mode coupling affects the eigenenergy splitting near an EP. Meanwhile, we find that the variations of the MNP radius can also achieve an EP, as shown in Figs. 2(c) and 2(d).

III. DETECTING AN EP WITH THE POWER SPECTRUM

In engineering the presence of an EP in the QE-MNP system, one of the important issues is to first verify its existence. To this end, we propose to utilize the power spectrum as a potential means to do so [55] since it is experimentally measurable and usually exhibits features which are theoretically well understood

As we will see in the following, the behavior of the power spectrum reflects the features of the EP, including the coalesce of eigenenergies and the drastic splitting of corresponding eigenenergies near the EP. However, we will also show the difficulty of limited visibility due to the broadening in the power spectrum caused by dissipation.

By definition, the power spectrum $S(\omega)$ is given by

$$S(\omega) = \frac{1}{\pi}\text{Re}\int_0^\infty d\tau \langle \hat{\sigma}_+^{(1)}(0)\hat{\sigma}_-^{(1)}(\tau)\rangle e^{i\omega\tau}, \quad (12)$$

where $\langle \hat{\sigma}_+^{(1)}(t)\hat{\sigma}_-^{(1)}(t+\tau)\rangle$ is the two-time correlation obtained by applying the quantum regression theorem to $\langle \hat{\sigma}_-^{(1)}(t)\rangle = \text{Tr}[\hat{\sigma}_-^{(1)}\rho(t)]$. The time evolution of the QE-MNP system density matrix $\rho(t)$ is governed by the master equation

$$\dot{\rho}(t) = \frac{i}{\hbar}[\rho(t), \hat{H}_{\text{eff}}] + \frac{\gamma_{QE}}{2}\mathcal{L}[\hat{\sigma}_-^{(1)}]\rho(t) \\ + \frac{\gamma_p}{2}\sum_{\beta=d,M}\mathcal{L}[\hat{a}_\beta]\rho(t) \quad (13)$$
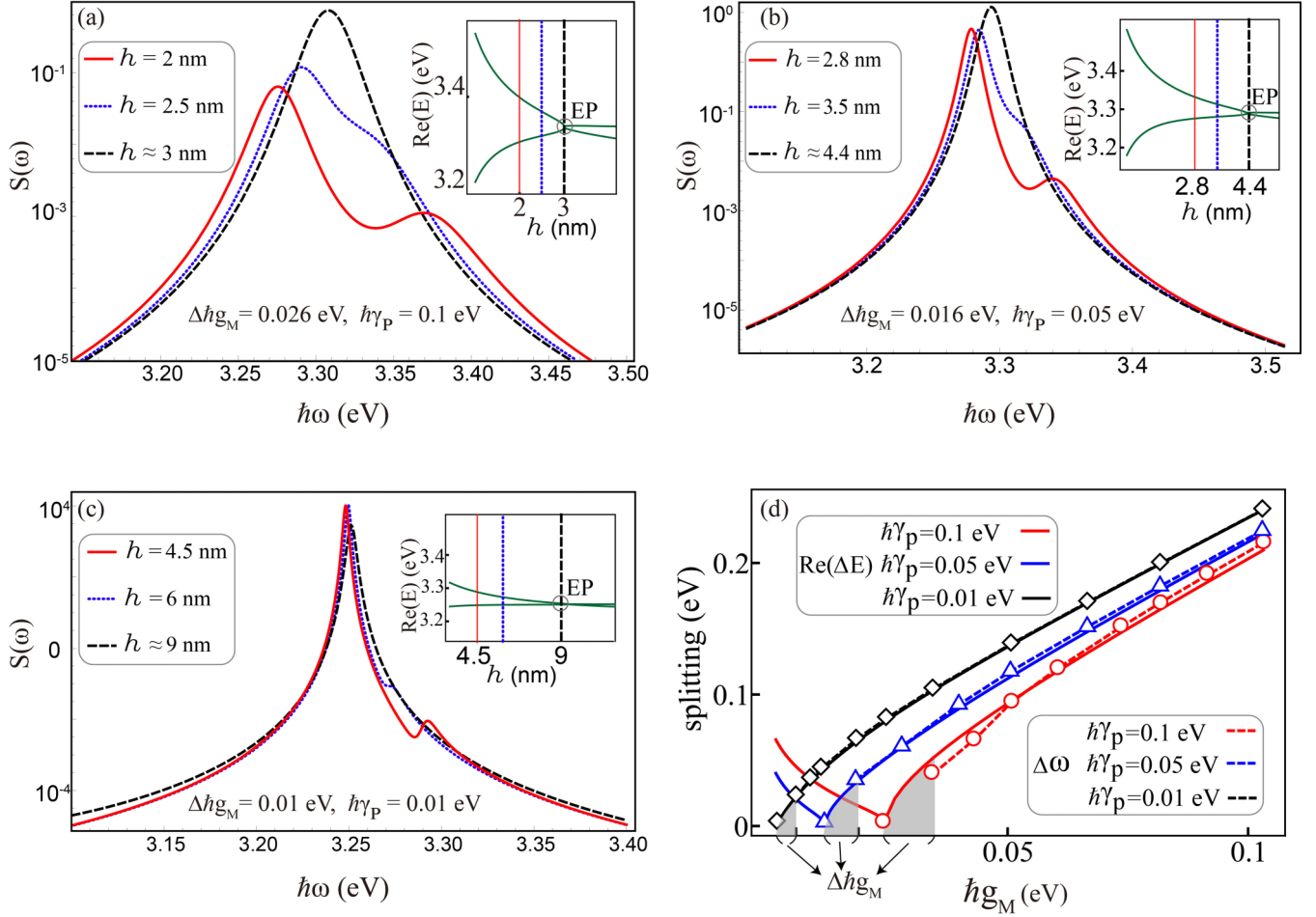
FIG. 3. (a) The power spectrum at different values of h with $\hbar\gamma_p = 0.1$ eV. For the case of $h \approx 3$ nm (black dashed curve), we can observe a single main peak, which is a consequence of the exceptional point, corresponding to the coalescence of eigenenergies shown in the inset. When moving the quantum emitter toward the metal nanoparticle at $h = 2.5$ nm (blue dotted curve), it reaches the critical splitting and defines an increment threshold $\triangle\hbar g_M = 0.026$ eV, i.e., the difference of the $\hbar g_M$ between $h \approx 3$ nm and $h = 2.5$ nm. When the quantum emitter is even closer to the metal nanoparticle at $h = 2$ nm (red solid curve), the splitting becomes more visible. In panels (b) and (c), in order to further investigate the relation between $\hbar\gamma_p$ and $\triangle\hbar g_M$, the value of $\hbar\gamma_p$ is reduced to 0.05 and 0.01 eV, respectively. The critical splittings occur at $h = 3.5$ and 6 nm, corresponding to the smaller thresholds $\triangle\hbar g_M = 0.016$ and 0.01 eV, respectively. Additionally, it should be noted that, in these panels, the $S(\omega)$ axis is shown on the logarithmic scale. (d) The real part of the splitting strength $\text{Re}(\triangle E)$ and the splitting in the power spectrum $\triangle\omega$ vs coupling strength $\hbar g_M$ with $\hbar\gamma_p = 0.1$ eV (red), 0.05 eV (blue), and 0.01 eV (black). The circle, triangle, and square dots on the dashed curves represent the numerical data points for $\triangle\omega$. $\text{Re}(\triangle E)$ rises drastically near the exceptional point. However, this behavior cannot be reflected in $\triangle\omega$ due to the broadening in the power spectrum. This leads to the undetectable regions marked in light gray; meanwhile, their widths equal to the threshold $\triangle\hbar g_M$.

with effective Hamiltonian

$$\hat{H}_{\text{eff}} = \hbar\omega_0\hat{\sigma}_{e_1,e_1}$$
$$+ \hbar \sum_{\beta=d,M} [\omega_\beta\hat{a}_\beta^\dagger\hat{a}_\beta + g_\beta(\hat{a}_\beta\hat{\sigma}_+^{(1)} + \hat{a}_\beta^\dagger\hat{\sigma}_-^{(1)})]. \quad (14)$$

The superoperator $\mathcal{L}$ is defined as

$$\mathcal{L}[\hat{o}]\rho(t) = \tfrac{1}{2}[2\hat{o}\rho(t)\hat{o}^\dagger - \rho(t)\hat{o}^\dagger\hat{o} - \hat{o}^\dagger\hat{o}\rho(t)].$$

As shown by the black dashed curve in Fig. 3(a), corresponding to the presence of an EP at $\hbar g_M \approx 0.025$ eV, $h \approx 3$ nm, and $\hbar\gamma_p = 0.1$ eV, the single main peak is the consequence of the EP. When we gradually move the QE towards the MNP, a splitting is present in the energy spectrum, as shown by the green curves in the inset of Fig. 3(a). However,

it should be noted that such splitting cannot be observed in the power spectrum until the QE is placed at $h = 2.5$ nm (blue dotted curve). This obfuscation is due to the broadening caused by dissipation. As a result of the dependence on h, the coupling strength g_M increases during the QE movement, and, consequently, we can define an increment threshold $\triangle\hbar g_M = 0.026$ eV, i.e., the difference of coupling strength between the emergence of an EP and the beginning of the splitting. As the QE is positioned at $h = 2$ nm (red solid curve), the splitting is even more notable since the increment in $\hbar g_M$ significantly exceeds the threshold $\triangle\hbar g_M$.

This implies that the visibility of the splitting in the power spectrum is an intuitive benchmark of its performance in detecting the EP. To enhance the visibility, it is critical to suppress the broadening in the power spectrum, such that the

increment in $\hbar g_M$ can more easily exceed the threshold $\triangle \hbar g_M$. Doing so helps us to rule out the region where the EP has been broken and, in turn, to pin down a smaller parameter range containing the EP, and hence improve the sensitivity.

As the dissipation is the origin of the broadening in the power spectrum, the former is responsible for the value of the threshold $\triangle \hbar g_M$ as well. In order to investigate the relation between $\hbar \gamma_p$ and $\triangle \hbar g_M$, we further reduce the value of $\hbar \gamma_p$ to 0.05 and 0.01 eV in Figs. 3(b) and 3(c), respectively. Following the same analysis as Fig. 3(a), we conclude that the corresponding $\triangle \hbar g_M = 0.016$ and 0.01 eV, respectively, in line with our explanation above.

To further schematically elaborate the intimate relation between $\hbar \gamma_p$ and $\triangle \hbar g_M$, in Fig. 3(d), we depict the real part of the splitting strength, Re($\triangle E$) (solid curves), of Eq. (9) and the visible splitting, $\triangle \omega$ (dashed curve), in the power spectrum, at $\hbar \gamma_p = 0.1$, 0.05, and 0.01 eV. Although the splitting in the energy spectrum around the EP is drastic, it cannot be reflected by $\triangle \omega$, due to the dissipation-induced broadening, as explained above. $\triangle \omega$ is finite only if the increment in $\hbar g_M$ exceeds $\triangle \hbar g_M$. This leads to the undetectable region, marked by the light gray areas in Fig. 3(d). It is clear that the smaller the γ_p the smaller the increment threshold $\triangle \hbar g_M$.

IV. EXCEPTIONAL POINTS INDUCED BY COLLECTIVE COUPLING TO SURFACE PLASMONS

When increasing the number of QEs near the MNP, one can expect a stronger interaction between the dipole mode of LSPs and the QEs compared to the previous case [56]. Hence, the strong-coupling regime between the LSPs and QEs can be easily reached by their collective coupling to the dipole mode, rather than to the pseudomode. In this regard, an EP is likely to be achieved via the collective coupling between the dipole mode and the QEs. We assume that there are N QEs arranged radially at h nm from the surface of the MNP with an identical dipole moment orientation of each i's QE $\vec{\mu}_i = (\mu_r, \mu_\theta, \mu_\phi)$ being parallel to the x axis, as illustrated in Fig. 4(a).

Transforming the dipole-dipole interaction

$$J_{ij} = \frac{1}{4\pi \epsilon_b}[\vec{\mu}_i \cdot \vec{\mu}_j/|\vec{r}_{ij}|^3 - 3(\vec{\mu}_i \cdot \vec{r}_{ij})(\vec{\mu}_j \cdot \vec{r}_{ij})/|\vec{r}_{ij}|^5]$$

into the effective detuning δ_J with identical distance r_{ij} between each adjacent QE, the interactions between the QEs and the LSPs can be described by the three-level non-Hermitian Hamiltonian:

$$H_{3\times3} = \begin{bmatrix} \omega_0 - i\frac{\gamma_{QE}}{2} + \delta_J & \sqrt{N}g_d & g_M \\ \sqrt{N}g_d & \omega_d - i\frac{\gamma_p}{2} & 0 \\ g_M & 0 & \omega_M - i\frac{\gamma_p}{2} \end{bmatrix}. \quad (15)$$

Note that a similar Hamiltonian was studied in Refs. [48,56] but not in the context of EPs. From the eigenvalue equations, one can obtain the energy spectra with the emergence of an EP by setting ten to twenty QEs in proximity to MNP as depicted in Figs. 4(b) and 4(c). Therefore, compared to the single-QE case, an EP here is mainly triggered by the collective coupling between the QEs and the dipole mode instead of the pseudomode. As we increase the number of the QEs, an EP occurs when the QEs are placed at a further distance h_{EP} from
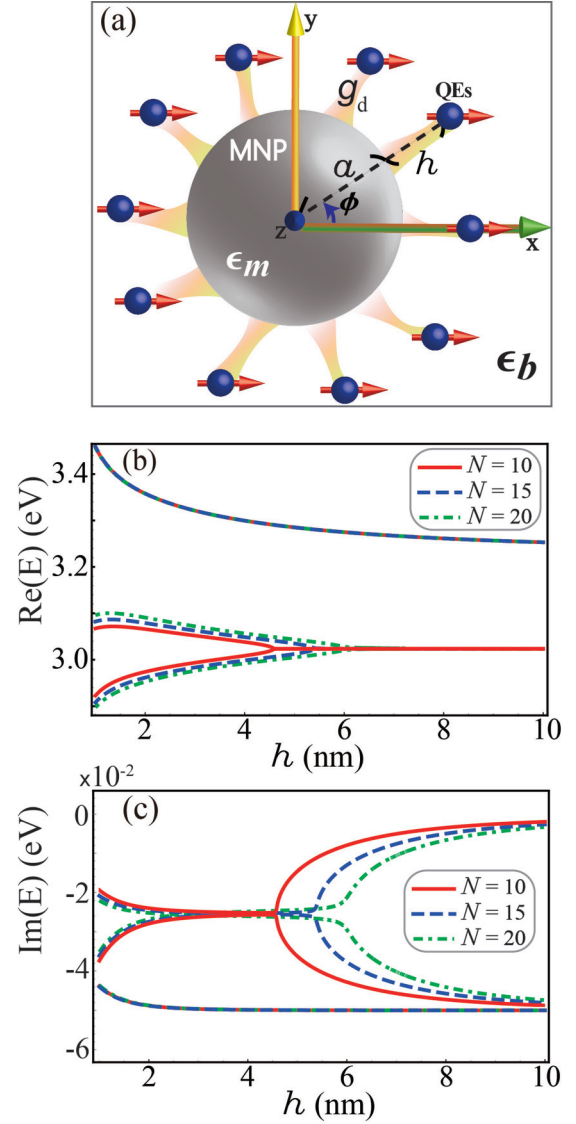

FIG. 4. (a) Schematic of N quantum emitters placed near the metal nanoparticle on the x-y plane at an identical distance h from the metal nanoparticle surface. The quantum emitters are separated from one another by $\phi = 2\pi/N$ along the $\vec{\phi}$ direction, with the dipole moment orientation being parallel to the x axis. (b), (c) The real (b) and imaginary (c) parts of the energy spectra as a function of h with $N = 10$ (red), $N = 15$ (blue), and $N = 20$ (green) quantum emitters. The observable shift of the exceptional point position, as well as the eigenenergy splitting, emerge when increasing the number of quantum emitters. The noticeable eigenenergy splittings result from an immense strength of the dipole-dipole interaction due to the close distances among quantum emitters. Note that by increasing the number of quantum emitters a stronger collective coupling to the dipole mode can be observed, such that the exceptional point occurs when the quantum emitters are placed at a longer distance h_{EP} with respect to the surface of the metal nanoparticle.

the surface of the MNP. However, if the composite system contains 20 QEs or even more, a complete energy splitting can occur due to the strong dipole-dipole interaction, such that the EP disappears. Therefore, there is a limit on the suitable number of the QEs to achieve an EP in the energy spectrum.

Besides the dipole-dipole interaction, the QEs coupled to the pseudomode also play an important role in the formation of eigenenergy splitting near an EP. In order to investigate how the coupling to the pseudomode affects the eigenenergy splitting, we make a comparison between different sizes of the MNPs coupled to ten QEs with the significant enhancement of the coupling to the pseudomode. The splitting emerges
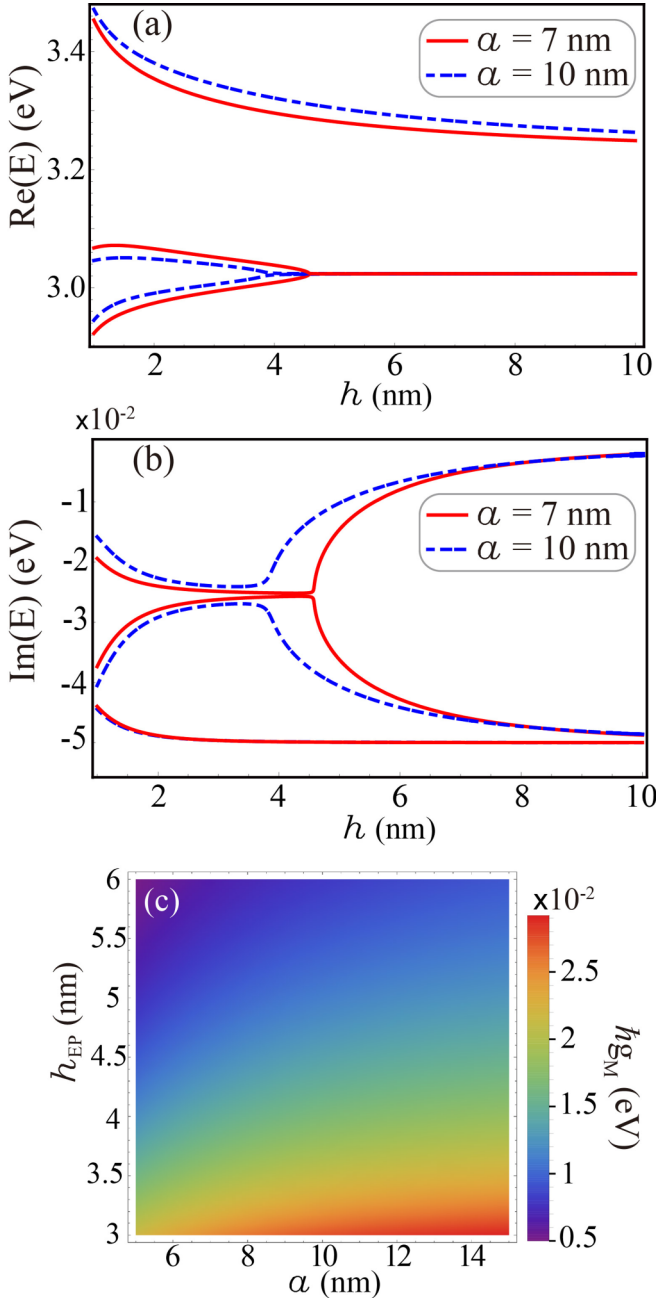

FIG. 5. (a), (b) Real (a) and imaginary (b) parts of the energy spectra as a function of distance h with the radius $a = 7$ (red solid) and $a = 10$ (blue dashed) when setting the number of quantum emitters $N = 10$. The larger the radius a, the smaller the distance h_{EP}, where an exceptional point emerges. (c) The eigenenergy splittings are triggered by an enhanced coupling to the pseudomode g_M with both increment of a and reduction in h_{EP}, which indicates that the region in blue color is suitable to perform the exceptional point.

while enlarging the MNP size from $a = 7$ to 10 nm, as shown in Figs. 5(a) and 5(b). This is because the enlargement of the MNP size is beneficial to enhance the coupling to the pseudomode.

Meanwhile, the distance h_{EP} for the occurrence of the EP becomes closer to the MNP. In this case, the coupling to the pseudomode can be enhanced, thereby increasing the splitting simultaneously. As shown in Figs. 5(c) and 5(d), the relation between h_{EP} and the radius a of the MNP can be described by an analytic form:

$$h_{EP} = -a + \left[\frac{6N\omega_d^3 (4\mu_r^2 + \mu_\theta^2 + \mu_\phi^2)}{\pi \epsilon_0 \omega_p^2 (\gamma_p - \gamma_{QE})^2} \right]^{\frac{1}{6}} \sqrt{a}. \tag{16}$$

Overall, the enlargement of the eigenenergies splitting at the position of an EP results from the enhancement of the coupling to the pseudomode, which can be caused by both increase of the MNP size and reduction in the distance h_{EP}.

V. DETECTING THE EXCEPTIONAL POINTS OF THE NUMEROUS QUANTUM EMITTERS CASE

Once again we can utilize the power spectrum to detect the presence of the EP in a system composed of numerous QEs coupled to LSPs. To do so we first consider the master equation of the QEs-MNP system:

$$\dot{\rho}(t) = \frac{i}{\hbar}[\rho(t), \hat{H}_{eff}] + \frac{\gamma_{QE}}{2}\mathcal{L}[\hat{\sigma}_-^{(c)}]\rho(t)$$
$$+ \frac{\gamma_p}{2} \sum_{\beta = d,M} \mathcal{L}[\hat{a}_\beta]\rho(t), \tag{17}$$

with effective Hamiltonian

$$\hat{H}_{eff} = \hbar(\omega_0 + \delta_J)\hat{\sigma}_+^{(c)}\hat{\sigma}_-^{(c)} + \hbar \sum_{\beta = d,M} \omega_\beta \hat{a}_\beta^\dagger \hat{a}_\beta$$
$$+ \hbar\sqrt{N}g_d(\hat{a}_d\hat{\sigma}_+^{(c)} + \hat{a}_d^\dagger\hat{\sigma}_-^{(c)})$$
$$+ \hbar g_M(\hat{a}_M\hat{\sigma}_+^{(c)} + \hat{a}_M^\dagger\hat{\sigma}_-^{(c)}), \tag{18}$$

where $\hat{\sigma}_+^{(c)}(\hat{\sigma}_-^{(c)})$ represents the raising (lowering) operator for the collection of QEs. Following the same procedure used in the single QE case, by calculating two-time correlations $\langle\hat{\sigma}_+^{(c)}(t)\hat{\sigma}_-^{(c)}(t+\tau)\rangle$, one can obtain the power spectrum:

$$S(\omega) = \frac{1}{\pi}\text{Re}\int_0^\infty d\tau \langle\hat{\sigma}_+^{(c)}(0)\hat{\sigma}_-^{(c)}(\tau)\rangle e^{i\omega\tau}.$$

Under suitable conditions, an EP is exhibited, i.e., $\sqrt{10}\hbar g_d \approx 0.025$ eV, $h \approx 4.6$ nm, $\hbar\gamma_p = 0.1$ eV, and we can observe only one main peak in the power spectrum as shown by the black dashed curve in Fig. 6(a), corresponding to the coalescence of eigenenergies, as shown by the green curves in the inset. When we move the QE toward the MNP, a drastic splitting is present in the energy spectrum. However, such splitting cannot be observed readily in the power spectrum since another peak merges into the main peak. Using the same approach as in the single QE case, the QEs should be placed at a close enough distance, i.e., $h = 3.5$ nm (blue dotted curve), in order to exceed the threshold of coupling to the dipole mode $\triangle\hbar g_d = 0.01$ eV. As the QE is positioned at $h = 2$ nm (red
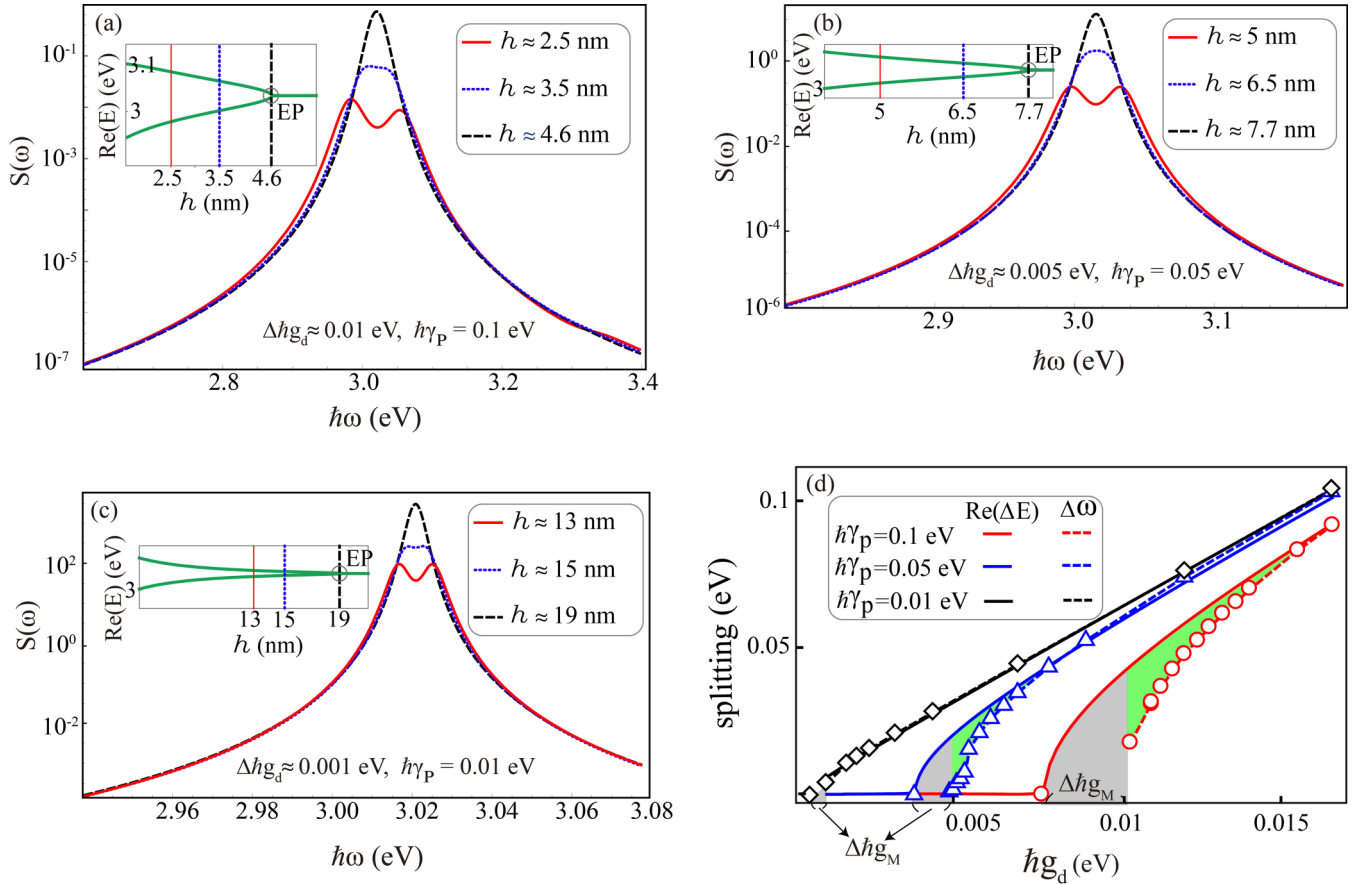
FIG. 6. (a) The power spectrum of ten quantum emitters for different values of h with $\hbar\gamma_p = 0.1$ eV. For the case of $h \approx 4.6$ nm (black dashed curve), the observation of a single main peak is a consequence of the exceptional point, corresponding to the coalescence of eigenenergies shown in the inset. When moving the quantum emitter toward the metal nanoparticle at $h = 3.5$ nm (blue dotted curve), a splitting starts to emerge from the broadening, which is the critical splitting, and here is defined as an increment threshold $\triangle\hbar g_d \approx 0.01$ eV. Moreover, when the quantum emitter is even closer to the metal nanoparticle at $h = 2.5$ nm (red solid curve), the splitting becomes more noticeable. In panels (b) and (c), in order to probe the relation between $\hbar\gamma_p$ and $\triangle\hbar g_d$, the value of $\hbar\gamma_p$ is reduced to 0.05 and 0.01 eV, respectively. The critical splittings occur at $h = 6.5$ and 15 nm, with respect to the smaller threshold $\triangle\hbar g_d = 0.005$ and 0.001 eV, correspondingly. Additionally, it should be noted that, in these panels, the $S(\omega)$ axis is shown on the logarithmic scale. (d) The real part of the splitting strength $\mathrm{Re}(\triangle E)$ and the splitting in the power spectrum $\triangle\omega$ vs coupling strength $\hbar g_d$ with $\hbar\gamma_p = 0.1$ eV (red), 0.05 eV (blue), and 0.01 eV (black). The circle, triangle, and square dots on the dashed curves represent the numerical data points for $\triangle\omega$. Although the $\triangle\omega$ near the exceptional point in the case of $\hbar\gamma_p = 0.1$ eV possesses a stronger dependence on $\hbar g_d$ than in the case of $\hbar\gamma_p = 0.05$ eV, it comes with the larger threshold $\triangle\hbar g_d$ (gray areas) in proximity to the exceptional point due to the wider broadening in the power spectrum. In addition, the green areas show that the $\triangle\omega$ in the power spectrum is smaller than the expected strength in the energy spectrum due to the larger $\hbar\gamma_p$.

solid curve), the splitting is more notable since the increment in $\hbar g_d$ significantly exceeds the threshold $\triangle\hbar g_d$.

Analogous to the single QE case, in order to explore the relation between $\hbar\gamma_p$ and $\triangle\hbar g_d$ for the ten QEs case, we then reduce the value of $\hbar\gamma_p$ to 0.05 and 0.01 eV in Figs. 6(b) and 6(c), corresponding to a threshold $\triangle\hbar g_d = 0.005$ and 0.001 eV, respectively. As expected, the QEs-MNP system with a smaller dissipation requires the smaller $\triangle\hbar g_d$ to observe the splitting.

Therefore, to further schematically analyze the relation between $\hbar\gamma_p$ and $\triangle\hbar g_d$, we plot the real part of the eigenenergies splitting near an EP, $\mathrm{Re}(\triangle E)$ (solid curves), and also the visible splitting, $\triangle\omega$ (dashed curve) in the power spectrum, at $\hbar\gamma_p = 0.1$, 0.05, and 0.01 eV, in Fig. 6(d). It is easier to identify the presence of an EP via the variation of g_d if the splitting near an EP is strongly dependent on g_d. This is

because, under the influence of larger dissipation, the QE-MNP system possesses more drastic splitting near the EP in the energy spectrum. However, for the larger dissipation case in the power spectrum, rather than the clearer observation of the drastic splitting, it actually comes with not only the larger threshold $\triangle\hbar g_d$ (gray area), but also a smaller splitting than the expected value in the energy spectrum (green area) due to the larger $\hbar\gamma_p$.

For this reason, how accurately the EP can be observed depends on how large of a strength of splitting one can detect near the EP in the power spectrum. Thus, the splitting ($\triangle\omega$) here is the information to be regarded as "the signal." The width of the main peak will obscure the ability to extract the required splitting. For convenience, the width of the main peak can be quantified using the full width at half maximum (FWHM), which has a relationship with $\hbar\gamma_p$ as depicted in
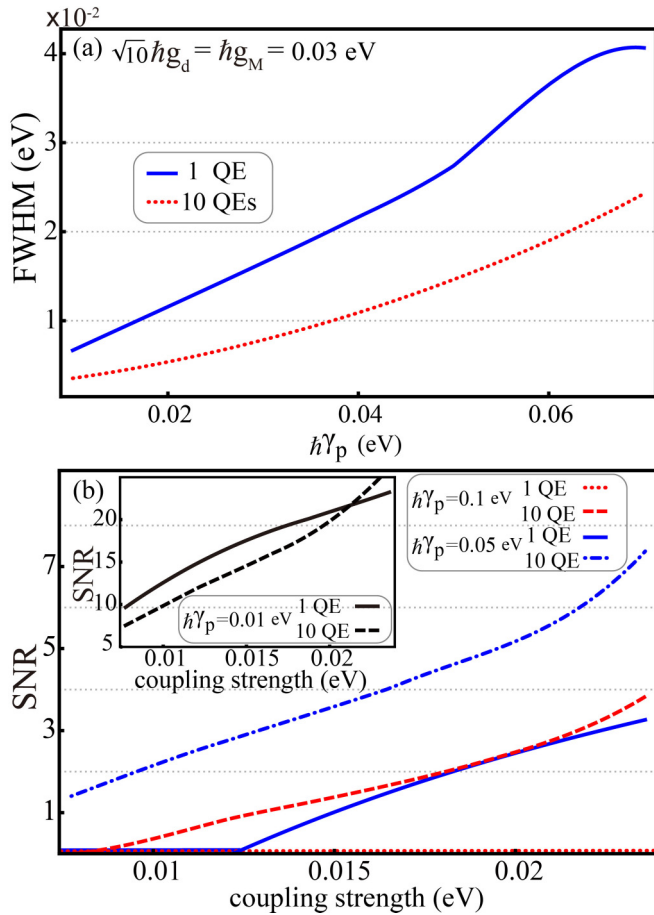
FIG. 7. (a) Variation in the FWHM vs dissipation $\hbar\gamma_p$. Solid blue and dotted red curves stand for the cases of a single quantum emitter and ten quantum emitters, respectively. The FWHM has positive correlation with $\hbar\gamma_p$. (b) SNR vs coupling strength of an individual quantum emitter. For the $\hbar\gamma_p = 0.01$ eV case shown in the inset, the SNR of the single quantum emitter case (solid black curve) is slightly higher than the ten quantum emitters case (dashed black curve) within the range of $\hbar g_{d(M)} = 0$ to 0.02 eV. In contrast, for the larger dissipation $\hbar\gamma_p = 0.05$ eV (solid and dot-dashed blue curves stand for the cases of a single quantum emitter and ten quantum emitters, respectively.) and $\hbar\gamma_p = 0.1$ eV (dotted and dashed red curves stand for the cases of a single quantum emitter and ten quantum emitters, respectively), the SNRs of the ten quantum emitters case are both higher than the single quantum emitter case.

Fig. 7(a). In this regard, we thus define a SNR, accounting for the splitting and FWHM, which quantifies the resolution of the power spectrum:

$$\text{SNR} = \frac{\triangle\omega}{\text{FWHM}}. \tag{19}$$

One can infer that the higher the SNR the better the resolution for detecting the EPs. Comparing the SNR of the single QE case to the ten QEs case, in terms of coupling strength, we find that although the SNR of a single QE case is slightly higher than in the ten QEs case for $\hbar\gamma_p = 0.01$ eV the SNR of the ten QEs case is conversely greater for both $\hbar\gamma_p = 0.05$ and 0.1 eV as shown in Fig. 7(b). Combining these results, a collection of

QEs possesses better SNR for larger system dissipation when considering the individual coupling strength of each QE.

VI. CONCLUSIONS

In conclusion, we have shown the emergence of EPs in open quantum systems composed of an MNP and a number of QEs. Surprisingly, an EP can stem from the coupling of different modes between a QE and LSPs. For the single-QE case, the formation of an EP mainly results from the coupling to a pseudomode, which becomes dominant when the distance between the QE and the MNP is shorter than 10 nm. However, the coupling to the dipole mode plays an important role in inducing the eigenenergy splittings near an EP. Subsequently, placing more QEs nearby the MNP triggers a collective coupling, which also induces an EP. Instead of the coupling to the dipole mode, the coupling to the pseudomode and the dipole-dipole interaction between QEs become important factors leading the splitting of eigenenergies near an EP. Therefore, with a proper balance between the quantum collective effect and the dipole-dipole interaction, using a number of QEs near the MNP not only relaxes the strong-coupling requirement for an individual QE, but also results in a more stable condition to generate exceptional points.

Furthermore, we have shown that EPs can be revealed in power spectra. Specifically, EPs correspond to frequency splitting in a power spectrum. We find that the system's dissipation sets a detection limit of observable splitting near an EP. The SNR analysis, accounting for frequency splitting and the system's dissipation, enables us to evaluate the accuracy of the observation of EPs. We conclude that a collection of QEs coupled to an MNP offers unique advantages in terms of a better SNR for the larger system's dissipation compared to that of a single QE.

APPENDIX: DERIVATIONS OF THE SPECTRAL DENSITY IN THE QUASISTATIC LIMIT

From the integrodifferential equation, given by Eq. (2), one can obtain the spectral density as follows [52]:

$$J(\omega) = \frac{\omega^2}{\pi \epsilon_0 c^2} \vec{\mu}_1 \cdot \mathrm{Im}[\widehat{G}(\vec{r}_1, \vec{r}_1, \omega)] \cdot \vec{\mu}_1, \qquad (A1)$$

where the Green's tensor $\widehat{G}(\vec{r}_1, \vec{r}_1, \omega)$ satisfies the boundary conditions [57]

$$\widehat{G}(\vec{r}_1, \vec{r}_1, \omega) = \widehat{G}_0(\vec{r}_1, \vec{r}_1, \omega) + \widehat{G}_{\mathrm{scatt}}(\vec{r}_1, \vec{r}_1, \omega). \qquad (A2)$$

Here, the full Green's tensor is composed of the unbounded dyadic Green's function $\widehat{G}_0(\vec{r}_1, \vec{r}_1, \omega)$ and the scattering dyadic Green's function $\widehat{G}_{\mathrm{scatt}}(\vec{r}_1, \vec{r}_1, \omega)$, which represent the vacuum contribution and an additional contribution of the multiple reflection and transmission waves, respectively. Given a silver MNP with the wave vector $k_m = \frac{\omega}{c}\sqrt{\epsilon_m}$ embedded in a homogeneous medium of wave vector $k_b = \frac{\omega}{c}\sqrt{\epsilon_b}$, the unbounded part of the dyadic Green's function, in terms of the spherical vector wave functions, is given by

$$\widehat{G}_0(\vec{r}_1, \vec{r}_1, \omega) = k_b \sum_{s=\pm} \sum_{n=0}^{\infty} \sum_{m=0}^{n} f_{mn} \big[\vec{M}_{mn}^{s(1)}(k_b r_1) \vec{M}_{mn}^{s}(k_b r_1)$$
$$+ \vec{N}_{mn}^{s(1)}(k_b r_1) \vec{N}_{mn}^{s}(k_b r_1) \big], \qquad (A3)$$

and the scattered part of the dyadic Green's function can be expanded as

$$\widehat{G}_{\mathrm{scatt}}(\vec{r}_1, \vec{r}_1, \omega) = k_b \sum_{s=\pm} \sum_{n=0}^{\infty} \sum_{m=0}^{n} f_{mn} \big[R_H \vec{M}_{mn}^{s(1)}(k_b r_1) \vec{M}_{mn}^{s(1)}(k_b r_1)$$
$$+ R_V \vec{N}_{mn}^{s(1)}(k_b r_1) \vec{N}_{mn}^{s(1)}(k_b r_1) \big], \qquad (A4)$$

where

$$f_{mn} = \frac{i}{4\pi}(2 - \delta_{m0}) \frac{2n+1}{n(n+1)} \frac{(n-m)!}{(n+m)!}.$$

Here, R_H and R_V represent the centrifugal reflection coefficients corresponding to the electric field of the TE and TM waves, respectively. We take the quasistatic limit into account due to the justified assumption that the distance between the MNP and QE is much smaller than the wavelength of the electromagnetic field ($k_b r_1 \ll 1$). Hence, the values of R_H and R_V are given by

$$R_H \approx \frac{i\pi a^{2n+3} k_b^{2n+1} \left(k_m^2 - k_b^2\right)}{2^{2n+4} \Gamma\left(n + \frac{3}{2}\right) \Gamma\left(n + \frac{5}{2}\right)}, \qquad (A5a)$$

$$R_V \approx \frac{i\pi(n+1)(k_b a)^{2n+1} \left(k_m^2 - k_b^2\right)}{2^{2n+1} \Gamma\left(n + \frac{1}{2}\right) \Gamma\left(n + \frac{3}{2}\right) \left[(n+1)k_b^2 + n k_m^2\right]} \quad (A5b)$$

Note that the spherical vector wave functions, $\vec{M}_{mn}^{s}(k_b r_1)$, $\vec{M}_{mn}^{s(1)}(k_b r_1)$ and $\vec{N}_{mn}^{s}(k_b r_1)$, $\vec{N}_{mn}^{s(1)}(k_b r_1)$, with $s = \pm$ corresponding to the TE and TM modes, respectively, can be defined as

$$\vec{M}_{mn}^{\pm}(k_b r_1) \approx -\frac{\sqrt{\pi}(k_b r_1)^n}{2^{n+1}\Gamma\left(n + \frac{3}{2}\right)} \left[\frac{m P_n^m(\kappa)}{\sin\theta_1} t_m^{\pm}(\phi_1) \hat{\theta} \pm \frac{dP_n^m(\kappa)}{d\theta_1} t_m^{\mp}(\phi_1) \hat{\phi} \right], \qquad (A6a)$$

$$\vec{M}_{mn}^{\pm(1)}(k_b r_1) \approx \frac{i 2^n m \Gamma\left(n + \frac{1}{2}\right)}{\sqrt{\pi}(k_b r_1)^{n+1}} \left[\frac{P_n^m(\kappa)}{\sin\theta_1} t_m^{\pm}(\phi_1) \hat{\theta} + \frac{dP_n^m(\kappa)}{d\theta_1} t_m^{\mp}(\phi_1) \hat{\phi} \right], \qquad (A6b)$$

$$\vec{N}_{mn}^{\pm}(k_b r_1) \approx \frac{\sqrt{\pi}(n+1)(k_b r_1)^{n-1} t_m^{\mp}(\phi_1)}{2^{n+1}\Gamma\left(n + \frac{3}{2}\right)} \left[n P_n^m(\kappa)\hat{r} + \frac{dP_n^m(\kappa)}{d\theta_1}\hat{\theta} - \frac{m P_n^m(\kappa)}{\sin\theta_1} \frac{t_m^{\pm}(\phi_1)}{t_m^{\mp}(\phi_1)}\hat{\phi} \right], \qquad (A6c)$$

$$\vec{N}_{mn}^{\pm(1)}(k_b r_1) \approx \frac{i 2^n n \Gamma\left(n + \frac{1}{2}\right) t_m^{\mp}(\phi_1)}{\sqrt{\pi}(k_b r_1)^{n+2}} \left[-(n+1) P_n^m(\kappa)\hat{r} + \frac{dP_n^m(\kappa)}{d\theta_1}\hat{\theta} - \frac{m P_n^m(\kappa)}{\sin\theta_1} \frac{t_m^{\pm}(\phi_1)}{t_m^{\mp}(\phi_1)}\hat{\phi} \right], \qquad (A6d)$$

where $t_m^{+}(\phi_1) = \sin(m\phi_1)$ and $t_m^{-}(\phi_1) = \cos(m\phi_1)$. $P_n^m(\kappa)$ is the associated Legendre polynomial with $\kappa = \cos\theta_1$, and $\Gamma(x)$ stands for the gamma function. Substituting all the spherical vector wave functions and the centrifugal reflection coefficients into the dyadic Green's function, one can obtain the elements of the full Green's tensor. One finds that only the three diagonal terms survive:

$$G^{rr}(\vec{r}_1, \vec{r}_1, \omega) = A + \sum_{n=0}^{\infty} BC_{nm} \left(\frac{n+1}{n+m-1} \right)^2, \qquad (A7a)$$

$$G^{\theta\theta}(\vec{r}_1, \vec{r}_1, \omega) = A(1 + \xi^2) + \sum_{n=0}^{\infty} \sum_{m=0}^{n} \mathcal{D}_{nm} B\big[C_{nm} P_{n+1}^m(0)^2 + C_{nm}' m^2 P_n^m(0)^2 \big], \qquad (A7b)$$

$$G^{\phi\phi}(\vec{r}_1, \vec{r}_1, \omega) = A(1 + \xi^2) + \sum_{n=0}^{\infty} \sum_{m=0}^{n} \mathcal{D}_{nm} B\big[C_{nm} m^2 P_n^m(0)^2 + C_{nm}' (n - m + 1)^2 P_{n+1}^m(0)^2 \big], \qquad (A7c)$$

where $A = ik_b/6\pi$, $\xi = k_b r_1/2$,

$$B = \frac{a^{2n+1}\left(k_b^2 - k_m^2\right)}{4\pi(a + h_1)^{2n+2}},$$

$$C_{nm} = \frac{n(n+m-1)^2}{(a+h_1)^2 k_b^2 \left[(n+1)k_b^2 + n k_m^2\right]},$$

and

$$C'_{nm} = \frac{a^2}{2n(n+1)[4n(n+2)+3]}.$$

Sequentially, the approximate Lorentzian form of the spectral density in Eq. (3) can be obtained by substituting Eqs. (A7a)–(A7c) into Eq. (A1).

[1] C. L. Degen, F. Reinhard, and P. Cappellaro, Quantum sensing, Rev. Mod. Phys. **89**, 035002 (2017).

[2] S. Pirandola, B. R. Bardhan, T. Gehring, C. Weedbrook, and S. Lloyd, Advances in photonic quantum sensing, Nat. Photonics. **12**, 724 (2018).

[3] A. P. Seyranian, O. N. Kirillov, and A. A. Mailybaev, Coupling of eigenvalues of complex matrices at diabolic and exceptional points, J. Phys. A: Math. Gen. **38**, 1723 (2005).

[4] U. Weiss, *Quantum Dissipative Systems*, 4th ed. (World Scientific, Singapore, 2012).

[5] R. El-Ganainy, K. G. Makris, M. Khajavikhan, Z. H. Musslimani, S. Rotter, and D. N. Christodoulides, Non-Hermitian physics and PT symmetry, Nat. Phys. **14**, 11 (2018).

[6] S. K. Özdemir, S. Rotter, F. Nori, and L. Yang, Parity-time symmetry and exceptional points in photonics, Nat. Mater. **18**, 783 (2019).

[7] G. Demange and E.-M. Graefe, Signatures of three coalescing eigenfunctions, J. Phys. A: Math. Theor. **45**, 025303 (2012).

[8] H.-K. Lau and A. A. Clerk, Fundamental limits and non-reciprocal approaches in non-Hermitian quantum sensing, Nat. Commun. **9**, 4320 (2018).

[9] H. Hodaei, A. U. Hassan, S. Wittek, H. Garcia-Gracia, R. El-Ganainy, D. N. Christodoulides, and M. Khajavikhan, Enhanced sensitivity at higher-order exceptional points, Nature (London) **548**, 187 (2017).

[10] W. Chen, S. K. Özdemir, G. Zhao, J. Wiersig, and L. Yang, Exceptional points enhance sensing in an optical microcavity, Nature (London) **548**, 192 (2017).

[11] W. Langbein, No exceptional precision of exceptional-point sensors, Phys. Rev. A **98**, 023805 (2018).

[12] B. Peng, S. K. Özdemir, F. Lei, F. Monifi, M. Gianfreda, G. L. Long, S. Fan, F. Nori, C. M. Bender, and L. Yang, Parity-time-symmetric whispering-gallery microcavities, Nat. Phys. **10**, 394 (2014).

[13] I. I. Arkhipov, A. Miranowicz, O. Di Stefano, R. Stassi, S. Savasta, F. Nori, and Şahin K. Özdemir, Scully-lamb quantum laser model for parity-time-symmetric whispering-gallery microcavities: Gain saturation effects and nonreciprocity, Phys. Rev. A **99**, 053806 (2019).

[14] H. Lü, S. K. Özdemir, L. M. Kuang, F. Nori, and H. Jing, Exceptional Points in Random-Defect Phonon Lasers, Phys. Rev. Appl. **8**, 044020 (2017).

[15] M. A. Miri and A. Alù, Exceptional points in optics and photonics, Science **363**, eaar7709 (2019).

[16] F. Minganti, A. Miranowicz, R. W. Chhajlany, and F. Nori, Quantum exceptional points of non-Hermitian Hamiltonians and Liouvillians: The effects of quantum jumps, Phys. Rev. A **100**, 062131 (2019).

[17] I. I. Arkhipov, A. Miranowicz, F. Minganti, and F. Nori, Quantum and semiclassical exceptional points of a linear system of coupled cavities with losses and gain within the Scully-Lamb laser theory, arXiv:1909.12276 (2019).

[18] C. E. Rüter, K. G. Makris, R. El-Ganainy, D. N. Christodoulides, M. Segev, and D. Kip, Observation of parity-time symmetry in optics, Nat. Phys. **6**, 192 (2010).

[19] A. Regensburger, C. Bersch, M.-A. Miri, G. Onishchukov, D. N. Christodoulides, and U. Peschel, Parity-time synthetic photonic lattices, Nature (London) **488**, 167 (2012).

[20] Z.-P. Liu, J. Zhang, S. K. Özdemir, B. Peng, H. Jing, X.-Y. Lü, C.-W. Li, L. Yang, F. Nori, and Y.-x. Liu, Metrology with $\mathcal{PT}$-Symmetric Cavities: Enhanced Sensitivity near the $\mathcal{PT}$-Phase Transition, Phys. Rev. Lett. **117**, 110802 (2016).

[21] A. U. Hassan, H. Hodaei, W. E. Hayenga, M. Khajavikhan, and D. N. Christodoulides, Enhanced sensitivity in parity-time-symmetric microcavity sensors, Adv. Photonics, SeT4C.3 (2015).

[22] H. Jing, S. K. Özdemir, X.-Y. Lü, J. Zhang, L. Yang, and F. Nori, $\mathcal{PT}$-Symmetric Phonon Laser, Phys. Rev. Lett. **113**, 053604 (2014).

[23] H. Jing, S. K. Özdemir, Z. Geng, J. Zhang, X.-Y. Lü, B. Peng, L. Yang, and F. Nori, Optomechanically-induced transparency in parity-time-symmetric microresonators, Sci. Rep. **5**, 9663 (2015).

[24] J. Zhang, B. Peng, S. K. Özdemir, Y.-x. Liu, H. Jing, X.-y. Lü, Y.-l. Liu, L. Yang, and F. Nori, Giant nonlinearity via breaking parity-time symmetry: A route to low-threshold phonon diodes, Phys. Rev. B **92**, 115407 (2015).

[25] F. Quijandría, U. Naether, S. K. Özdemir, F. Nori, and D. Zueco, $\mathcal{PT}$-symmetric circuit QED, Phys. Rev. A **97**, 053846 (2018).

[26] Y. Choi, S. Kang, S. Lim, W. Kim, J.-R. Kim, J.-H. Lee, and K. An, Quasieigenstate Coalescence in an Atom-Cavity Quantum Composite, Phys. Rev. Lett. **104**, 153601 (2010).

[27] S.-B. Lee, J. Yang, S. Moon, S.-Y. Lee, J.-B. Shim, S. W. Kim, J.-H. Lee, and K. An, Observation of an Exceptional Point in a Chaotic Optical Microcavity, Phys. Rev. Lett. **103**, 134101 (2009).

[28] J. Wiersig, Sensors operating at exceptional points: General theory, Phys. Rev. A **93**, 033809 (2016).

[29] J. Zhu, S. K. Özdemir, L. He, and L. Yang, Controlled manipulation of mode splitting in an optical microcavity by two Rayleigh scatterers, Opt. Express **18**, 23535 (2010).

[30] C. Dembowski, H.-D. Gräf, H. L. Harney, A. Heine, W. D. Heiss, H. Rehfeld, and A. Richter, Experimental Observation of the Topological Structure of Exceptional Points, Phys. Rev. Lett. **86**, 787 (2001).

[31] C. Dembowski, B. Dietz, H.-D. Gräf, H. L. Harney, A. Heine, W. D. Heiss, and A. Richter, Encircling an exceptional point, Phys. Rev. E **69**, 056216 (2004).

[32] B. Dietz, T. Friedrich, J. Metz, M. Miski-Oglu, A. Richter, F. Schäfer, and C. A. Stafford, Rabi oscillations at exceptional points in microwave billiards, Phys. Rev. E **75**, 027201 (2007).

[33] Y.-L. Liu, R. Wu, J. Zhang, S. K. Özdemir, L. Yang, F. Nori, and Y.-x. Liu, Controllable optical response by modifying the gain and loss of a mechanical resonator and cavity mode in an optomechanical system, Phys. Rev. A **95**, 013843 (2017).

[34] K. Ding, G. Ma, M. Xiao, Z. Q. Zhang, and C. T. Chan, Emergence, Coalescence, and Topological Properties of Multiple Exceptional Points and Their Experimental Realization, Phys. Rev. X **6**, 021007 (2016).

[35] B. Alfassi, O. Peleg, N. Moiseyev, and M. Segev, Diverging Rabi Oscillations in Subwavelength Photonic Lattices, Phys. Rev. Lett. **106**, 073901 (2011).

[36] B. Zhen, C. W. Hsu, Y. Igarashi, L. Lu, I. Kaminer, A. Pick, S.-L. Chua, J. D. Joannopoulos, and M. Soljačić, Spawning rings of exceptional points out of Dirac cones, Nature (London) **525**, 354 (2015).

[37] T. Gao, E. Estrecho, K. Y. Bliokh, T. C. H. Liew, M. D. Fraser, S. Brodbeck, M. Kamp, C. Schneider, S. Höfling, Y. Yamamoto, F. Nori, Y. S. Kivshar, A. G. Truscott, R. G. Dall, and E. A. Ostrovskaya, Observation of non-Hermitian degeneracies in a chaotic exciton-polariton billiard, Nature (London) **526**, 554 (2015).

[38] A. Kodigala, T. Lepetit, and B. Kanté, Exceptional points in three-dimensional plasmonic nanostructures, Phys. Rev. B **94**, 201103(R) (2016).

[39] S. Sunada, Large Sagnac frequency splitting in a ring resonator operating at an exceptional point, Phys. Rev. A **96**, 033842 (2017).

[40] H. Jing, S. K. Özdemir, H. Lü, and F. Nori, High-order exceptional points in optomechanics, Sci. Rep. **7**, 3386 (2017).

[41] B. Peng, Ş. K. Özdemir, S. Rotter, H. Yilmaz, M. Liertzer, F. Monifi, C. M. Bender, F. Nori, and L. Yang, Loss-induced suppression and revival of lasing, Science **346**, 328 (2014).

[42] J. Zhang, B. Peng, S. K. Özdemir, K. Pichler, D. O. Krimer, G. Zhao, F. Nori, Y.-x. Liu, S. Rotter, and L. Yang, A phonon laser operating at an exceptional point, Nat. Photonics. **12**, 479 (2018).

[43] M. S. Tame, K. R. McEnery, S. K. Özdemir, J. Lee, S. A. Maier, and M. S. Kim, Quantum plasmonics, Nat. Phys. **9**, 329 (2013).

[44] R. Chikkaraddy, B. de Nijs, F. Benz, S. J. Barrow, O. A. Scherman, E. Rosta, A. Demetriadou, P. Fox, O. Hess, and J. J. Baumberg, Single-molecule strong coupling at room temperature in plasmonic nanocavities, Nature (London) **535**, 127 (2016).

[45] D. Pile, Exceptional plasmonics, Nat. Photonics. **11**, 24 (2017).

[46] G.-Y. Chen, N. Lambert, C.-H. Chou, Y.-N. Chen, and F. Nori, Surface plasmons in a metal nanowire coupled to colloidal quantum dots: Scattering properties and quantum entanglement, Phys. Rev. B **84**, 045310 (2011).

[47] S. Savasta, R. Saija, A. Ridolfo, O. Di Stefano, P. Denti, and F. Borghese, Nanopolaritons: Vacuum Rabi splitting with a single quantum dot in the center of a dimer nanoantenna, ACS Nano **4**, 6369 (2010).

[48] A. Delga, J. Feist, J. Bravo-Abad, and F. J. Garcia-Vidal, Quantum Emitters Near a Metal Nanoparticle: Strong Coupling and Quenching, Phys. Rev. Lett. **112**, 253601 (2014).

[49] N. Zhou, M. Yuan, Y. Gao, D. Li, and D. Yang, Silver nanoshell plasmonically controlled emission of semiconductor quantum dots in the strong coupling regime, ACS Nano **10**, 4154 (2016).

[50] T. Neuman, R. Esteban, D. Casanova, F. J. García-Vidal, and J. Aizpurua, Coupling of molecular emitters and plasmonic cavities beyond the point-dipole approximation, Nano Lett. **18**, 2358 (2018).

[51] H. T. Dung, L. Knöll, and D.-G. Welsch, Spontaneous decay in the presence of dispersing and absorbing bodies: General theory and application to a spherical cavity, Phys. Rev. A **62**, 053804 (2000).

[52] A. González-Tudela, P. A. Huidobro, L. Martín-Moreno, C. Tejedor, and F. J. García-Vidal, Reversible dynamics of single quantum emitters near metal-dielectric interfaces, Phys. Rev. B **89**, 041402(R) (2014).

[53] S. Hughes, M. Richter, and A. Knorr, Quantized pseudomodes for plasmonic cavity QED, Opt. Lett. **43**, 1834 (2018).

[54] S. Franke, S. Hughes, M. Kamandar Dezfouli, P. Trøst Kristensen, K. Busch, A. Knorr, and M. Richter, Quantization of Quasinormal Modes for Open Cavities and Plasmonic Cavity Quantum Electrodynamics, Phys. Rev. Lett. **122**, 213901 (2019).

[55] A. Ridolfo, O. Di Stefano, N. Fina, R. Saija, and S. Savasta, Quantum Plasmonics with Quantum Dot-Metal Nanoparticle Molecules: Influence of the Fano Effect on Photon Statistics, Phys. Rev. Lett. **105**, 263601 (2010).

[56] A. Delga, J. Feist, J. Bravo-Abad, and F. J. Garcia-Vidal, Theory of strong coupling between quantum emitters and localized surface plasmons, J. Opt. **16**, 114018 (2014).

[57] L.-W. Li, P.-S. Kooi, M.-S. Leong, and T.-S. Yee, Electromagnetic dyadic Green's function in spherically multilayered media, IEEE Trans. Microwave Theory Tech. **42**, 2302 (1994).